Analyst

ROYAL SOCIETY OF CHEMISTRY

PAPER

View Article Online
View Journal | View Issue

Cite this: *Analyst*, 2025, **150**, 386

Witnessing a discrete microdroplet freezing event *via* real-time electrochemical monitoring of solution temperature†

Philip J. Kauffmann,‡[a] Cristian A. Blanco-Combariza‡[a] and Jeffrey E. Dick *[a,b]

Temperature monitoring has immediate relevance to many areas of research, from atmospheric environmental studies to biological sample and food preservation to chemical reactions. Here, we use a triple-barrel electrode to provide temperature readouts in bulk solution and microdroplets, as well as electrochemically monitor freezing events in a microdroplet. Using this method, we are able to identify distinct characteristics of a freezing aqueous droplet (supercooling, ice formation beginning and end, temperature change, and thawing) with greater temporal resolution than a standard thermocouple and without the use of microscopy. By correlating the amperometric signal change caused by alterations in the diffusion coefficient of the electrochemical system in response to temperature changes, we can calculate the instantaneous temperature at our electrode, as well as the physical behavior of ice formation and expansion. Our results suggest that these electrochemical techniques can provide real-time monitoring of the physical processes involved in aqueous temperature change and ice nucleation events. Here, we employ a novel technique using triple-barrel electrodes to provide temperature readouts in bulk solution and microdroplets, as well as electrochemically monitor freezing events in a microdroplet. Because ice nucleation spans many research fields, it is important to have a variety of tools that can be used to better understand these frozen systems. Our data shows that electrochemistry can provide real-time information on the thermal properties of aqueous environments, and these types of measurements can be extended to microdroplets. The electrochemical signal details all the significant moments in a droplet freezing event, allowing us to use electrochemistry as a stand-alone tool for monitoring freezing events with excellent temporal and spatial resolution.

Received 9th September 2024,
Accepted 4th December 2024

DOI: 10.1039/d4an01200c

rsc.li/analyst

Introduction

Accurate temperature monitoring is a concern in a myriad of fields. From running chemical reactions and biological assays[1] to microbiological growth and industrial processes,[2] temperature monitoring allows researchers and industry professionals to control experimental conditions and synthetic parameters.[3,4] One area of interest involving temperature monitoring is electrochemistry.[9] Many of the processes involved in electrochemical reactions and electroanalytics are closely tied to the temperature of the system in question,[11] with many mass transfer effects being significantly temperature dependent.[9] As a system's temperature can directly affect an electrochemical signal,[10,12] we suspect an electrochemical signal should act as a direct temperature readout.[12,34] To explore these effects, we have turned to electrochemical techniques that offer sensitive and real-time monitoring capabilities.[8,33] We designed a system of generating different temperatures to study electrochemical systems as a function of temperature.

This system was based on the Peltier effect[6] and used commercially available thermoelectric components. Thermoelectric effects are a series of physical phenomena discovered in the early 19th century, precipitated by the 1821 discovery of potential differences between two distinct metals in contact under different temperature conditions by Thomas Seebeck.[5,6] The dubbed Seebeck effect still has use as the operating principle behind thermocouple-based temperature monitoring apparatus.[7] In 1834, Jean Charles Athanase Peltier discovered that current applied to systems of distinct materials generates a temperature gradient usable in heating and refrigeration.[5–7] The Peltier effect has many real-world applications as a compact, solid-state form of heat transfer.[7]

Electrochemistry has long been involved in the study of low temperature systems.[9] Most of these low temperature studies

[a]*Department of Chemistry, Purdue University, West Lafayette, IN, 47907, USA. E-mail: jdick@purdue.edu*
[b]*Elmore Family School of Electrical and Computer Engineering, Purdue University, West Lafayette, IN 47907, USA*

†Electronic supplementary information (ESI) available. See DOI: https://doi.org/10.1039/d4an01200c

‡Indicates equal contribution.

sought to measure the formation of radical ions as reaction intermediates.[10,11] Under these conditions, the average lifetime of these species is increased dramatically.[10] Additionally, electrochemistry is used to probe physical processes such as corrosion in extreme temperature conditions.[11] Electrochemical setups have several advantages for exploring reactions and chemical systems.[8] Low instrumental cost, fast measurement speed, and high sensitivity combine to make electrochemistry an attractive analytical technique. One of the downfalls of these techniques is the instrumental setup.[13]

Electrochemistry measures electrical signals detected on a series of electrodes. The standard electrochemical cell involves three distinct electrodes.[8] The Working electrode acts as the driving force for any redox reactions occurring in the system, the Counter electrode closes the circuit generated by the cell, and the reference electrode acts as a standard for the system and reactions.[14] While powerful, this setup requires a relatively large volume to work. Although Working and Counter electrodes can be found in sizes down to the nanometer scale, the reference electrode is hard to miniaturize, which limits the size of the systems that the electrodes can probe.[13]

In response, our lab has designed and produced a probe that combines all three electrodes into a single capillary.[13] This triple-barreled electrode has channels for the working, counter, and reference electrodes, bringing the total size of the electrochemical cell down to the micrometer scale.[14] Using this probe in conjunction with a commercially available thermoelectric component allowed us to monitor electrochemical traces of well-behaved analytes at distinct temperatures, as well as allowing us to observe the electrochemical signals produced at distinct phase change conditions, specifically the freezing of the aqueous medium as the temperature drops below 0 °C.

These electrochemical traces have shown many signals of interest, including distinct areas where the system cools and even the specific point where the aqueous droplet freezes completely.[17] The electrochemical signal can help us better understand the kinetics of ice nucleation and the physical process of freezing as we approach the point of complete freezing.[15,33]

While freezing kinetics is an important area of inquiry,[32–36] it is essential to note that electrochemical systems will have difficulty probing ice nucleation as a simulation of in-atmosphere particles.[17,37] The presence of the probes within the droplets can act as nucleation sites for ice,[15] which would not be present in real-world systems.[34–36] Atmospheric particles typically present with microscopic imperfections[17] or contaminations[18] that act as sources of ice formation known as nucleation sites.[37] This process is known as homogenous nucleation and typically occurs in pure water at 235 K.[16] The presence of a probe in the system is enough to induce ice nucleation at these temperatures.[18] However, the surface the studied water droplets are placed upon has enough surface imperfections to act as a nucleation site.[15] For the purposes of this study, the probe itself does not impact the nucleation kinetics in a significant way.[17]

We present a detailed study of electrochemical temperature sensing using amperometric techniques with thermoelectric components as temperature controls. We investigate the correlation between temperature and electrochemical signal. We explore the effects temperature has on amperometry and use electrochemical measurements to monitor phase transitions in real-time. Our experimental setup allows for precise and rapid temperature control on our system, lending itself well to electrochemical temperature studies in the future. Through rigorous experimentation and analysis, we aim to advance the understanding of electrochemical temperature sensing and provide insights into the practical implementation of this approach in various fields. The findings of this study have implications for improving the analytical scope of electrochemical techniques. Subsequent studies will explore additional applications for these phenomena, including studying cryopreservation viability in cells.[15]

Materials and methods

Reagents and materials

Gallium (99.9% trace metal basis) was obtained from Sigma Aldrich. Potassium chloride (KCl) salt was obtained from Thermo Fisher Scientific. Potassium ferrocyanide trihydrate (99+% for analysis) and potassium ferricyanide (99+%, ACS reagent) were purchased from Acros Organics. Ultrapure water (Millipore Milli-Q, 18.2 MΩ cm) was used to make aqueous solutions and microdroplets. Platinum wire (99.95% metals basis, d = 25 μm) for triple-barrel electrode fabrication was purchased from Thermo Scientific. Silver wire (d = 0.25 mm, hard, 99.9% metals basis) was obtained from Thermo Scientific. 22AWG Silicone Hook Up Wire (OD: 1.7 mm) – 22 Gauge Stranded Tinned Copper Wire with Silicone Insulation, 6 Colors (Black, Red, Yellow, Green, Blue, White) 23 ft/7 m Each, Hook Up Wire Kit from Plusivo was used for making electrical connection in the triple-barrel electrodes. Borosilicate triple barrel glass capillaries (1.0/0.50 mm OD/ID) were purchased from Sutter Instrument (Novato, California). A rotary RZ-6 vacuum pump was purchased from Vacuubrand. Vacuum tubes were purchased from Fisher Scientific and New Age Industries. A propane torch was used to seal the platinum wires within the borosilicate glass, and the propane was obtained from Bernzomatic. The lab stand jack was purchased from Amazon. Images were taken with a Park Systems 50–500× LED USB Digital Microscope. Electrochemical experiments were performed using a CHI model 6284E potentiostat (CH Instruments, Austin, Texas) with a three-electrode cell. The cooling setup was sourced primarily through online retailers (Amazon). The cooler setup involved four main components. The thermoelectric module was a commercially available TEC1-12706 Thermoelectric Cooler. The temperature data for the experiments was logged on a Gain Express 88598 Digital 4 Channel K-type Thermocouple Thermometer. The water-cooling segment consisted of a Mavel Star Submersible Mini Water Pump connected *via* 5/16-inch internal diameter vinyl tubing to a DIYHz Aluminum Water Cooling Block. The contacts between components were thermally connected by the

application of Wakefield Thermal Solution-brand Type 120 Thermal Joint Compound.

Triple barrel electrode (TBE) fabrication

A small length (2–3 cm) of Pt wire (d = 25 μm) was threaded into each channel of a triple barrel borosilicate glass capillary. A vacuum line was attached to the opposite end of the capillary, and the vacuum was allowed to run for 2 minutes before sealing the capillary around the Pt wires with a propane torch. After sealing, the vacuum line was removed. Electrical wire was cut and a section the length of the electrode was stripped. The tip of the exposed electrical wire was then dipped in liquid gallium and threaded into one of the channels of the triple barrel capillary. An identical electrical wire was cut and threaded into a second channel. The third channel was filled with 1 M KCl solution by a microneedle (Hamilton 1701RN, 10 μL, 32 ga/2″ removable needle), and then a chloride-coated, silver wire was inserted into the channel. The wires were secured into place with hot glue, leaving a small length of wire still exposed at the end of each channel for connection to the potentiostat. The tip of the triple barrel electrode was then polished (first with sandpaper, then with alumina powder) to expose the Pt wires, until a clean CV was obtained, and then used to make all electrochemical measurements discussed herein.

Bulk temperature monitoring setup

Two holes were drilled into the cap of the 20 mL vial near the center. The electrode and thermocouple were inserted through the holes and positioned so that the tips of each probe were level with and near each other close to the center of the vial (Fig. 1). The vial containing the redox solution was held by a ring-stand clamp. The ice or hot water bath was switched out alternatively by placing them on the lab stand jack and raising it until the water level of the bath was higher than the solution level of the vial (*i.e.*, fully submerged). Amperometric and temperature measurements continued even while replacing the hot and ice water baths.

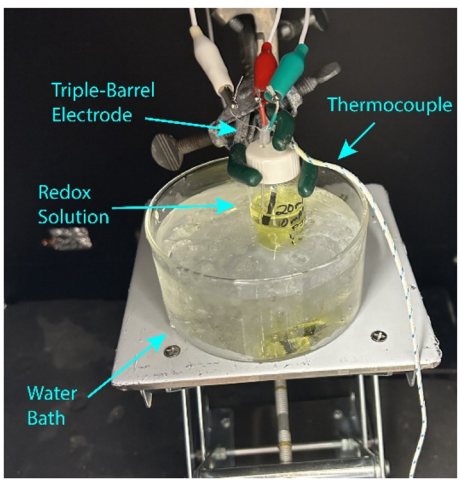

Fig. 1 Experimental setup for the bulk temperature monitoring experiments. The bath was supported on a lab stand jack for ease of replacing the water bath without disturbing the electrochemical sensor. The thermocouple and electrode were positioned to be at the same height within the redox solution and roughly at the center of the vial.

Microdroplet setup

A thermoelectric Peltier cooler was integrated into a cooling system to regulate the temperature of the experimental media. The Peltier cooler consisted of a water-cooled aluminum block at the base, through which ice water was pumped, maintaining the surface at 0 °C. Above that, a series of commercially available TEC-12706 thermoelectric (TEC) modules were placed, with a thin layer of electronic-grade thermal compound acting as a thermal conductor between the TECs and the block. To reduce the electrical noise in our measurements, the setup was covered in a makeshift Faraday cage, consisting of grounded aluminum foil. Finally, to ensure thermal conductivity and electrical insulation, a layer of ceramic was placed above the Faraday cage. This system allowed the TEC to be pre-cooled to approximately 0C, which increased the temperature range the experimental system could achieve.

Power was supplied to the TEC system through means of an adapted power cord. This provided electrical power with a magnitude of 18 V and 6 A. These values are within the specifications for the chosen TECs, albeit close to the maximum rating for these modules. Variable cooling was achieved by applying electrical current through a variable power supply. For most experiments, our interest lay in cooling the system as quickly as possible to the lowest temperature, therefore the power cord was the preferred electrical supply.

An aqueous droplet was dispensed onto the top layer of ceramic of the Peltier system. The triple-barrel electrode and thermocouple were taped together so that the ends of each probe were level. They were then attached to a micropositioner and lowered into the water droplet before making electrochemical and temperature measurements. The data collection for each device (and the USB camera) was started simultaneously in order to correlate all data.

Results and discussion

Bulk temperature monitoring

To begin understanding the capabilities of our sensor to probe thermodynamic properties, the triple-barrel electrode was inserted into a 20 mL solution of 10 mM hexacyanoferrate II/III in 1 M KCl (Fig. 1). A thermocouple was also inserted into the vial and adjusted so that the tips of the two probes were level. Baths containing either ice water (~5 °C) or hot water (~45 °C) were alternatively introduced to cool or heat the vial. By using amperometry, our triple-barrel electrode provides a direct readout of the current. Using eqn (1) [19] and (2),[20]

$$i = 4nFDCr \quad (1)$$

$$D = k_B T/(6\pi\eta R) \quad (2)$$

we can convert the current into temperature, and plot temperature as a function of time. In eqn (1), i is the current, n is the number of electrons in the reaction (1), F is Faraday's constant (96 485 C mol^{-1}), D is the diffusion coefficient of the redox species (substituted into eqn (1) from eqn (2)), C is the concentration of the redox species (10 mM), and r is the electrode radius (12.5 μm). In eqn (2), D is the diffusion coefficient of the redox species, k_B is Boltzmann's constant (1.38×10^{-23} m^2 kg s^{-1} K^{-1}), T is the temperature being solved for, η is the solution viscosity (approximately 0.00115 kg m^{-1} s^{-1} (ref. 21)), and R is the hydrodynamic radius of the redox molecule (310 pm (ref. 22)). An example calculation is shown in eqn (S1).† While the solution viscosity, η, is dependent on temperature, we assume that this variable remains constant, such that the majority of influence from temperature change will affect the diffusion coefficient. Additionally, while this event can be explained by considering diffusion of the species, under extreme temperature gradients, convection driven by these gradients may initially contribute to the redistribution of molecules. However, given the temperature match in Fig. 2, this effect seems to be minimal but could explain slight differences. This allows us to only have one variable, T, and so plot the current data as a function of temperature over time and compensated for with a simple correction factor. By overlaying this readout with the direct temperature measurements from our thermocouple, we can compare the direct readout of temperature from the thermocouple and the indirect readout of temperature from the triple-barrel electrode. As seen in Fig. 2, the two traces correlate very closely. These traces do deviate slightly, and we attribute these differences to the fact that the two methods are fundamentally measuring different phenomena, although they are both influenced by temperature as a function of time. The electrochemical measurement is primarily a readout of the change in mass transport of the redox species, while the thermocouple is measuring the voltage caused by the difference in the thermal expansion coefficients between the two metals of the thermocouple probe. While the measurements are different, we show below that the values obtained from the two methods are quite similar. The small geometry of the microelectrode ensures diffusion-dominated mass transport, as spherical diffusion profiles at this scale minimize the influence of convection, even with moderate temperature gradients. While additional factors like convection and viscosity changes could enhance model accuracy, the current approach provides a reliable representation of the system's behavior, as demonstrated in Fig. 2.

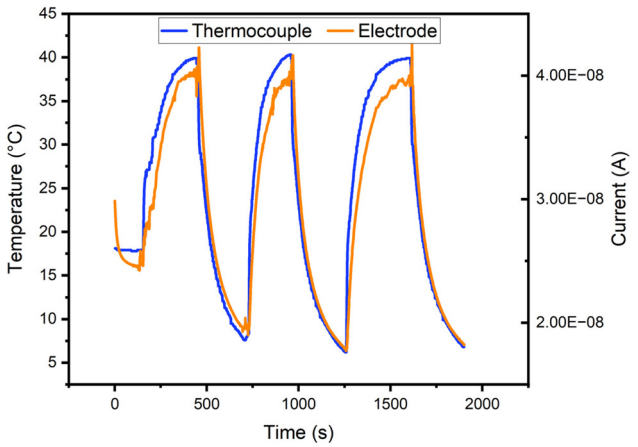

Fig. 2 An overlay of the direct readout of temperature change *via* a thermocouple (blue trace); and a direct readout of the current change *via* a triple-barrel electrode (TBE, orange trace). The temperature is cycled several times, using warm (~45 °C at the start) and ice (~0 °C) water baths, respectively.

The temperature of the 10 mM hexacyanoferrate(II/III) solution is cycled several times using an ice bath or a hot bath. To help quantify the accuracy, we compared the readouts of the two different methods once the temperature changes began (*i.e.*, 155–1900 s). Using the values at each second for the two methods, the average difference between the two methods was determined to be 0.5 °C.

While the solution viscosity is also affected by temperature, we leave this term constant and assume that the change in current is dominated by mass transfer as the molecules increase or decrease in thermodynamic energy. Simulations were conducted over a range of viscosity values spanning three orders of magnitude. These tests revealed no noticeable impact on diffusion-controlled current, indicating that the system's response is largely unaffected by viscosity changes in this range. This supports the reliability of temperature measurements, suggesting that the electrochemical readout reflects temperature more directly than viscosity. At present, our model does not take into account viscosity gradients, which may give rise to slight differences, which can be observed in Fig. 2, when measuring with well-established techniques. As a result, we use a small correction factor in the calculation (eqn (S1)†). For each cycle, there is a rapid spike in current as the hot bath is switched for an ice bath. This event can be explained by considering the diffusion of the species. As an extreme temperature gradient is introduced, the hot redox molecules move quickly to achieve equilibrium, creating a rapid flux detected at the electrode surface. This does not happen as noticeably when the hot bath is reintroduced after the temperature cools down, because although there is an introduction of a large temperature gradient, the molecules at cold temperatures cannot respond as quickly to the new temperature gradient, and so there is not a significant increase in flux at the electrode surface. Regardless, this event is very rapid, and the current continues to track with the independent temperature readout. Thus, extreme temperature changes in the system do not significantly interfere with the readout of the system and its ability to track temperature change. To ensure accurate temperature calibration, steady-state conditions may offer a more stable reference point than transient conditions, given potential delays in the thermocouple's response. However, as observed in Fig. 2, the close tracking between the thermocouple and the electrochemical measurement across a relevant temperature range, highlights the relationship between temperature and diffusion for electro-

chemical measurements. Future studies may further refine calibration methods to enhance accuracy.

Confined volume temperature measurements

The previous experiment demonstrates how amperometry can be used as an accurate readout of temperature to a single °C. However, given the enormous attention recently on curious chemistry in small volumes,[23–31] one may wish to make temperature-dependent measurements inside a small volume. The nature of the setup makes it difficult to investigate temperatures at which ice nucleation would occur. Further, as mentioned previously, we are interested in investigating small volumes. Thus, we modify the setup by using a cooling system to freeze microdroplets, as described above and shown in Fig. 3. We pipette a microliter droplet onto the cooling system and use a micropositioner to insert the triple-barrel electrode into the droplet. We also taped a thermocouple to the side of the triple-barrel electrode, such that the tips of both probes were effectively at the same height within the microdroplet. The cooling system also includes a pump through which ice water (~0 °C) flows through the setup.

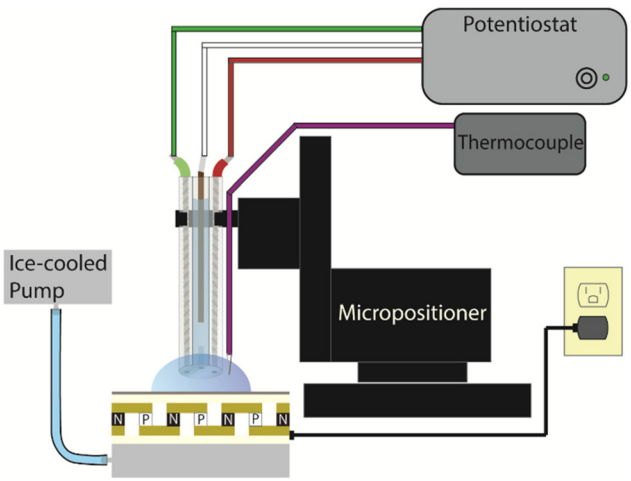

Fig. 3 Illustration of the setup used to measure ice freezing events with electrochemistry. The triple barrel electrode and thermocouple are inserted into an aqueous droplet (30 μL).

In this system, we can employ similar methods as before, using amperometry to monitor the temperature change of a solution; however, in this case, we monitor the freezing of a 30 μL droplet of 50 mM ferrocyanide in 0.5 M KCl.

Fig. 4A shows an overlay of current as a function of temperature and the direct readout of temperature from the thermocouple. Specific characteristics can be correlated to specific events, as indicated in Fig. 4B. A full video of the freezing and thawing of the microdroplet can be found in the ESI.†

Similar to before, we use the starting temperature of the system as the "zero" point, to determine how accurately the triple-barrel electrode monitors temperature change from this starting temperature. While the overlay in Fig. 4 correlates very closely, there are some noticeable differences between the traces. To begin, the electrode and thermocouple probes are in open air and are then introduced into the droplet at 15 seconds (Fig. 4Ai and Bi). This results in a sharp increase in current at the electrode as the oxidation of ferrocyanide begins, and a slight drop in temperature at the probe. The current reaches a steady state, as expected, immediately after the introduction of the probe into the droplet. At 45 seconds (not pictured), the cooling system is turned on, and the droplet experiences a rapid decrease in temperature. This also results in a sharp decline of current as the redox molecules

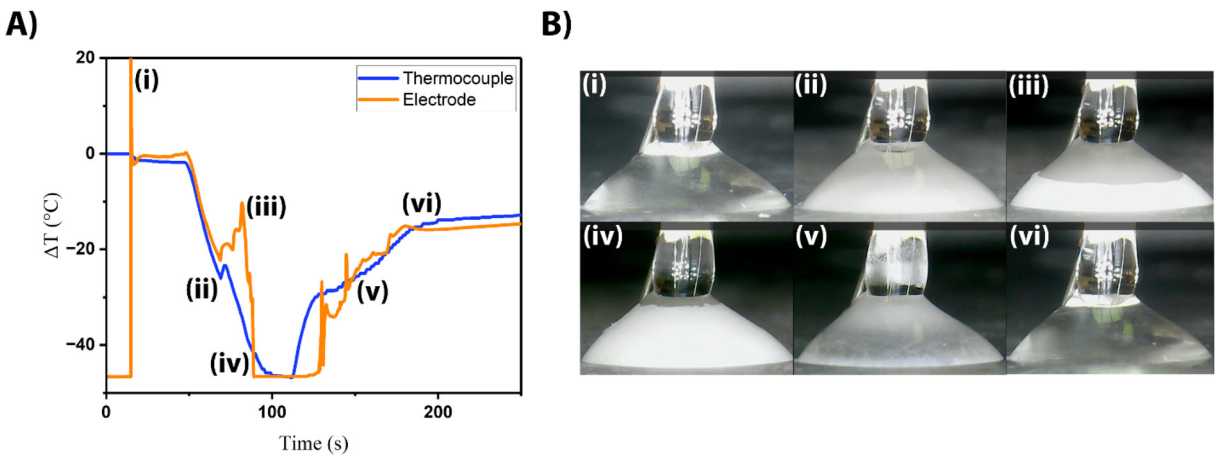

Fig. 4 Comparison of the direct temperature readout (thermocouple, panel A blue trace) to the indirect temperature readout (electrode, panel A orange trace). The indirect method with the triple-barrel electrode shows several characteristics: the electrode enters the microdroplet, beginning the oxidation of ferrocyanide which quickly reaches a steady state current (Bi); the supercooling event causes the droplet to become cloudy and releases a small amount of heat (Bii); ice nucleation starts at the base of the droplet and propagates up towards the electrode (Biii); ice growth reaches the probe surface, inhibiting further oxidation of ferrocyanide (Biv); the droplet is thawing but ice is still present, jostling the electrode surface (Bv); the droplet has completely thawed, no ice remains (Bvi). Electrochemical conditions: WE: 25 μm Pt disk *vs.* Ag/AgCl, 50 mM ferrocyanide in 0.5 M KCl in 30 μL droplet.

lose thermodynamic energy and so begin to diffuse to the electrode surface more slowly. At 69 seconds (Fig. 4Aii and Bii), the system experiences the supercooling effect, which causes a slight increase in the temperature of the overall system and diffusion of the redox molecules. Despite this brief interruption, the system continues to rapidly decrease in temperature as ice growth progresses upward through the droplet. As freezing approaches the electrode from 69–82 seconds (Fig. 4Aiii and Biii), it appears that the rising "ice wall" seems to violently perturb the molecules within, causing a dramatic increase in current signal. The ice wall appears to reach the electrode surface at 90 seconds (Fig. 4Aiv and Biv), effectively freezing all molecules and halting the redox signal. The cooling pump and Peltier are turned off at 110 seconds, after which the microdroplet begins to thaw, rapidly at first (Fig. 4Av and Bv). The amperometry is unsteady with the occasional spike in current, indicating that the thawing during this time period is tumultuous until the ice thaws and the droplet warms at a slower rate (Fig. 4Avi and Bvi). Other runs with similar characteristics can be seen in Fig. S1,† and these characteristics remain even at different concentrations of supporting electrolyte. The thawing portion of the transients are more difficult to interpret (although it appears to be somewhat tumultuous as the amperometric signal spikes dramatically at several points), and so the electrochemical characteristics during the freezing event will be focused on. From this data, we can see that the electrochemical data is a rich source of specific details about the freezing process, many of which are lost when only considering the temperature data from the thermocouple.

The average rate of cooling for these trials from the moment the cooling system is turned on to when the droplet is fully frozen depends on the salt concentration. Table 1 shows the average time between turning the cooling system on and the flash freeze event, as well as the average overall time between the cooling system being turned on and the signal turn-off (*i.e.*, fully frozen microenvironment). From this, we can determine that the average rate of temperature change increases with decreasing salt concentrations.

As expected, droplets with higher salt concentrations generally freeze at a slower rate and take more time. The trend is easier to see when the overall time of the freezing events is considered (columns two and three). The trend in freezing rate is not as clear at salt concentrations of 0.5 M and 0.375 M, but this may be due to an outlier in the data (Table S1†). Regardless, the trend stands that microdroplets with lower salt concentrations freeze more quickly.

Table 1 Effect of salt concentrations on the freezing rates of microdroplets (n = 3)

Salt concentration (M)	Average time to flash freeze (s)	Average time to signal off (s)	Average rate of T change (°C s^{-1})
0.5	21.8 ± 1.7	45.7 ± 1.6	0.76 ± 0.13
0.375	19.7 ± 3.0	43.1 ± 4.1	0.74 ± 0.07
0.25	17.4 ± 4.1	37.7 ± 2.9	0.80 ± 0.03
0	14.0 ± 0.6	33.9 ± 0.6	0.87 ± 0.01

Importantly, electrochemistry gives information about the system that cannot be discerned with just the thermocouple (Fig. 4A). The thermocouple shows that as ice growth progresses throughout the droplet, the temperature decreases, quickly at first (45–95 seconds) and then slowly (95–110 seconds). From this information, one might guess that ice has completely nucleated throughout the droplet at approximately 95 seconds, since this is when the rate of temperature seems to change most significantly. This would be incorrect, as the ice has reached the probe surface 5 seconds sooner at the 90 seconds mark. This is exactly what is indicated by the electrochemistry. The amperometry shows that there is a rapid decrease in temperature (Fig. 4A, 45–90 s) and that there is a very tumultuous transient that correlates with the supercooling event of the microdroplet (Fig. 4Aii). There is then an even more dramatic decrease in signal to where the amperometric signal shuts off at 90 seconds (Fig. 4Aiv). These timestamps correlate with observations from microscopy when the ice wall appears to reach the probe. As mentioned before, this signal shut-off occurs roughly 5 seconds before the temperature readout from the thermocouple might indicate that the microenvironment is frozen. The electrochemical shut-off is only dependent on the environment immediately around the electrode tip, regardless of the location of the probe within the droplet. This indicates that a probe like this can be easily coupled with a micropositioner to evaluate particular positions within a microenvironment.

These results also show that electrochemical probes can accurately indicate the temperature conditions of microenvironments in real time, and with greater temporal precision than a typical thermocouple. With only a single probe, the amperometric i–t trace can readily identify all the characteristics (*i.e.*, supercooling, beginning and completion of ice growth, and the temperature of the microenvironment) that would otherwise take multiple methods (microscopy and a temperature probe) to determine. While a somewhat large, 30 μL does not require advanced microscopy techniques, our method as described here can readily be extended to nanoelectrodes which could be used to probe environments of even smaller size, or specific sites within a microenvironment.

From our data, we suggest that kinetic information of the ice growth might be able to be extracted. As the ice wall approaches the surface of the electrode, the ice inhibits the flux of the redox molecules and interrupts the steady state diffusion layer of the redox molecules. This character can be discerned from the amperometric traces as the electrochemical signal shuts off. To highlight this, Fig. 5 shows triplicate electrochemical measurements of a 30 μL droplet of 50 mM ferrocyanide in 0.375 M KCl.

The inset graph highlights that the signal shut-off is not immediate. Rather, there is a decay-like curve at these points, indicating a rapid, but not instantaneous, signal shut-off. These decay-like curves, when overlayed on top of each other, are reproducible (Fig. S5†). Intuitively, as the ice approaches the electrode surface, the diffusion layer will be interrupted. We suggest that these decay-like curves show the final

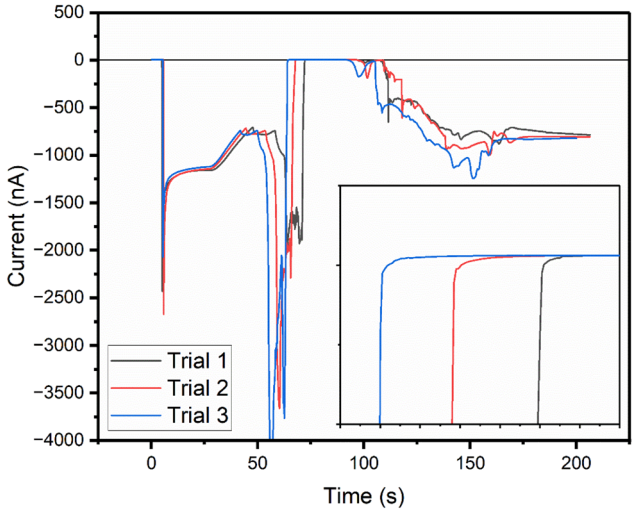

Fig. 5 Amperometric *i*–*t* curves with an inset graph from 62–76 seconds showing the electrochemical signal shut-off in a decay-like fashion. The line across the inset graph is 0 A.

moments of the diffusion layer before the viscosity dramatically increases and inhibits all flux to the electrode surface. It should be noted that although the current does not stop exactly at 0 amps, this current is the same as before the electrochemical probe is inserted into the droplet at t = 0–15 s; thus, there is no oxidation of ferrocyanide occurring. An interesting characteristic of the decay curve geometry is the similarity between it and the signal output of a scanning electrochemical microscope (SECM) in negative feedback mode.[33,34,36] Additional work on the subject is being carried out to properly characterize this similarity.

A rough rate of ice growth can be extracted from microscopy by measuring the ice wall with Image J as ice propagates upwards through the microdroplet. For the amperometric experiments in Fig. 5, we measured the average rate of ice growth across the three experiments to be 116 ± 4 μm s^{-1}. The analysis can be found in Fig. S6.† To corroborate this rate, we created a COMSOL Multiphysics simulation (see ESI†) to replicate the ice nucleating up the droplet to the electrode surface. We simulated this by using a non-flux boundary (representing the ice wall) approaching the electrode surface at the rate we estimated from microscopy. In Fig. S7,† we show three simulations of amperometric traces, each with a different viscosity spanning three orders of magnitude for the phase change from liquid to solid. In each case, the current response shows a decay-like signal and simulations with higher viscosity approach zero current more rapidly than lower viscosity simulations. This corroborates the idea that there is a relationship between the signal shut-off and the viscosity change as ice nucleates throughout the droplet.

A final consideration when probing the heterogeneous ice nucleation regime is how the measurement system itself (*i.e.*, the triple-barrel electrode or the thermocouple) may be affecting the nucleation. The surface of our Peltier system, where the droplet is pipetted, provides an obvious source for the nucleation to begin, as indicated by our observations (see ESI Fig. S2†). If the nucleation began at our probe, it could inhibit our ability to make measurements. However, the origin of nucleation and growth of the "ice wall" indicates that the probe does not act as a nucleation site. As we investigate smaller droplets in the future, this may become a significant concern. Additionally, the nature of the probe itself may introduce uncertainty in the microenvironment surrounding the electrode. Heat transfer effects, differing amongst materials, could have an impact on the temperature detection of the system. Additional studies, particularly involving the effect of specific electrode materials on the electrochemical measurements may be required to further validate the robustness of this technique.

Conclusion

Here we present a novel method for monitoring freezing events in microenvironments using a triple-barrel, electrochemical probe. Because ice nucleation spans many research fields, it is important to have a variety of tools that can be used to better understand these frozen systems. Our data shows that electrochemistry can provide real-time information on the thermal properties of aqueous environments, and these types of measurements can be extended to microdroplets. The electrochemical signal details all of the significant moments in a droplet freezing event, from tracking the temperature drop to the supercooling event, to total crystallization of the droplet at the electrode surface, to droplet thawing. Finally, this data can be combined with Multiphysics finite element models to correlate ice growth kinetics, microdroplet viscosity, and electrochemical data. All together, these experiments show that electrochemistry can work as a stand-alone tool for monitoring freezing events with excellent temporal and special resolution.

Author contributions

PJK and CABC performed all experiments. PJK and CABC wrote the manuscript. JED supervised all aspects of the research presented. All authors have given approval to the final version of the manuscript.

Data availability

Data are available upon request from the corresponding author.

Conflicts of interest

There are no conflicts of interest to declare.

Acknowledgements

The authors would like to acknowledge support from the Chemical Measurement and Imaging Program in the National Science Foundation Division of Chemistry under grant CHE 2403964. The authors would also like to acknowledge Azaria Wagner for his collaboration and support involving the analysis of relevant simulations.

References

1 J. Maynard, R. van Hooidonk, C. D. Harvell, C. M. Eakin, G. Liu, B. L. Willis, M. L. Groner, A. Dobson, S. F. Heron, R. Glenn, K. Reardon and J. D. Shields, Improving Marine Disease Surveillance Through Sea Temperature Monitoring, Outlooks and Projections, *Philos. Trans. R. Soc., B*, 2016, **371**(1689), 20150208, DOI: 10.1098/rstb.2015.0208.

2 D. Zou, C. Du, T. Liu and W. Li, Effects of Temperature on the Performance of the Piezoelectric-Based Smart Aggregates Active Monitoring Method for Concrete Structures, *Smart Mater. Struct.*, 2019, **28**(3), 035016, DOI: 10.1088/1361-665x/aafe15.

3 M. K. Lim, Y. Li, C. Wang and M.-L. Tseng, Prediction of Cold Chain Logistics Temperature Using a Novel Hybrid Model Based on the Mayfly Algorithm and Extreme Learning Machine, *Ind. Manage. Data Syst.*, 2022, **122**(3), 819–840, DOI: 10.1108/imds-10-2021-0607.

4 Z. Xiao, C. Liu, T. Zhao, Y. Kuang, B. Yin, R. Yuan and L. Song, Review—Online Monitoring of Internal Temperature in Lithium-Ion Batteries, *J. Electrochem. Soc.*, 2023, **170**(5), 057517, DOI: 10.1149/1945-7111/acd586.

5 H. Adachi, K.-I. Uchida, E. Saitoh and S. Maekawa, Theory of the Spin Seebeck Effect, *Rep. Prog. Phys.*, 2019, **76**(3), 036501, DOI: 10.1088/0034-4885/76/3/036501.

6 S. Parveen, S. V. Vedanayakam and R. P. Suvarna, Thermoelectric Power Generation with Load Resistance Using Thermoelectric Generator, *Int. J. Res. Appl. Sci. Eng. Technol.*, 2017, **5**(IX), 862–870, DOI: 10.22214/ijraset.2017.9126.

7 A. Azhar, M. F. Lathifah, A. Doyan, S. Susilawati and L. S. Hudha, Digital-Based Thermoelectric Generator, *J. Phys.:Conf. Ser.*, 2022, **2165**(1), 012033, DOI: 10.1088/1742-6596/2165/1/012033.

8 C. Schotten, T. P. Nicholls, R. A. Bourne, N. Kapur, B. N. Nguyen and C. E. Willans, Making Electrochemistry Easily Accessible to the Synthetic Chemist, *Green Chem.*, 2020, **22**(11), 3358–3375, DOI: 10.1039/d0gc01247e.

9 R. P. V. Duyne and C. Reilley, Low-Temperature Electrochemistry. I. Characteristics of Electrode Reactions in the Absence of Coupled Chemical Kinetics, *Anal. Chem.*, 1972, **44**(1), 142–152, DOI: 10.1021/ac60309a026.

10 M. A. Edwards, D. A. Robinson, H. Ren, C. G. Cheyne, C. S. Tan and H. S. White, Nanoscale Electrochemical Kinetics & Dynamics: The Challenges and Opportunities of Single-Entity Measurements, *Faraday Discuss.*, 2018, **210**, 9–28, DOI: 10.1039/c8fd00134k.

11 S. Ching, J. T. McDevitt, S. R. Peck and R. Murray, Liquid Phase Electrochemistry at Ultralow Temperatures, *J. Electrochem. Soc.*, 1991, **138**(8), 2308–2315, DOI: 10.1149/1.2085966.

12 C. Schulzke, Temperature Dependent Electrochemistry—A Versatile Tool for Investigations of Biology Related Topics, *Dalton Trans.*, 2009, **34**, 6683, DOI: 10.1039/b904361f.

13 P. J. Kauffmann, N. L. Walker, V. Gupta and J. E. Dick, Triple-Barrel Ultramicroelectrodes for Multipurpose, Submilliliter Electroanalysis, *Anal. Chem.*, 2023, **95**(22), 8411–8416, DOI: 10.1021/acs.analchem.3c00735.

14 N. A. Park, G. L. Glish and J. E. Dick, Investigating Electrosprayed Droplets Using Particle-Into-Liquid Sampling for Nanoliter Electrochemical Reactions, *J. Am. Soc. Mass Spectrom.*, 2023, **34**(2), 320–327, DOI: 10.1021/jasms.2c00338.

15 Z. He, K. Liu and J. Wang, Bioinspired Materials for Controlling Ice Nucleation, Growth, and Recrystallization, *Acc. Chem. Res.*, 2018, **51**(5), 1082–1091, DOI: 10.1021/acs.accounts.7b00528.

16 S. A. Zielke, A. K. Bertram and G. N. Patey, Simulations of Ice Nucleation by Kaolinite (001) with Rigid and Flexible Surfaces, *J. Phys. Chem. B*, 2016, **120**(8), 1726–1734, DOI: 10.1021/acs.jpcb.5b09052.

17 G. D. Soria, J. R. Espinosa, J. Ramirez, C. Valeriani, C. Vega and E. Sanz, A Simulation Study of Homogeneous Ice Nucleation in Supercooled Salty Water, *J. Chem. Phys.*, 2018, **148**(22), DOI: 10.1063/1.5008889.

18 P. A. Alpert, J. Y. Aller and D. A. Knopf, Ice Nucleation from Aqueous NaCl Droplets with and Without Marine Diatoms, *Atmos. Chem. Phys.*, 2011, **11**(12), 5539–5555, DOI: 10.5194/acp-11-5539-2011.

19 A. J. Bard, L. R. Faulkner and H. S. White, *Electrochemical Methods: Fundamentals and Applications*, John Wiley and Sons Ltd, 3rd edn, 2022, p. 219.

20 A. J. Bard, L. R. Faulkner and H. S. White, *Electrochemical Methods: Fundamentals and Applications*, John Wiley and Sons Ltd, 3rd edn, 2022, pp. 195.

21 J. Kestin, M. Sokolov and W. A. Wakeham, Viscosity of Liquid Water in the Range -8 °C to 150 °C, *J. Phys. Chem. Ref. Data*, 1978, **7**, 941, DOI: 10.1063/1.555581.

22 W. R. Fawcett, M. Hromadova, G. A. Tsilina and R. R. Nazmutdinov, The Role of Charge Distribution in the Reactant and Product in Double Layer Effects for Simple Heterogeneous Redox Reactions, *J. Electroanal. Chem.*, 2001, **498**(1–2), 93–104.

23 K. J. Vannoy, I. Lee, K. Sode and J. E. Dick, Electrochemical Quantification of Accelerated FADGDH Rates in Aqueous Nanodroplets, *Proc. Natl. Acad. Sci. U. S. A.*, 2021, **118**(25), e2025726118.

24 L. Krushinski and J. Dick, Direct Electrochemical Evidence Suggests That Aqueous Microdroplets Spontaneously Produce Hydrogen Peroxide, *Proc. Natl. Acad. Sci. U. S. A.*, 2024, **121**(12), e2321064121.

25 B. R. Layman and J. E. Dick, Through-Space Electrochemiluminescence Reveals Bubble Forces at Remote Phase Boundaries, *J. Am. Chem. Soc.*, 2024, **146**(1), 707–713.
26 J. Li, Y. Xia, X. Song and R. N. Zare, Continuous Ammonia Synthesis From Water and Nitrogen via Contact Electrification, *Proc. Natl. Acad. Sci. U. S. A.*, 2024, **121**(4), e2318408121.
27 X. Song, C. Basheer, Y. Xia, J. Li, I. Abdulazeez, A. A. Al-Saadi, M. Mofidfar, M. A. Suliman and R. N. Zare, One-step Formation of Urea from Carbon Dioxide and Nitrogen Using Water Microdroplets, *J. Am. Chem. Soc.*, 2023, **145**(47), 25910–25916.
28 D. T. Holden, N. M. Morato and R. G. Cooks, Aqueous Microdroplets Enable Abiotic Synthesis and Chain Extension of Unique Peptide Isomers from Free Amino Acids, *Proc. Natl. Acad. Sci. U. S. A.*, 2022, **119**(42), e2212642119.
29 K. J. Vannoy and J. E. Dick, Oxidtion of Cysteine by Electrogenerated Hexacyanoferrate(III) in Microliter Droplets, *Langmuir*, 2022, **38**(39), 11892–11898.
30 B. R. Layman and J. E. Dick, Phase-Resolved Electrochemiluminescence with a Single Luminophore, *J. Phys. Chem. Lett.*, 2023, **14**(36), 8151–8156.
31 S. Voci, T. B. Clarke and J. E. Dick, Abiotic Microcompartments Form When Neighboring Droplets Fuse: An Electrochemiluminescence Investigation, *Chem. Sci.*, 2023, **14**, 2336–2341.
32 A. Baranski and S. Hot Microelectrodes, *Anal. Chem.*, 2002, **74**(6), 1294–1301, DOI: **10.1021/ac015659h**.
33 Z. Zhao, K. C. Leonard and A. Boika, Hot-Tip Scanning Electrochemical Microscopy: Theory and Experiments Under Positive and Negative Feedback Conditions, *Anal. Chem.*, 2019, **91**(4), 2970–2977, DOI: **10.1021/acs.analchem.8b05192**.
34 H. Pan, H. Zhang, J. Lai, X. Gu, J. Sun, J. Tang and T. Jin, Integration of thermocouple microelectrode in the scanning electrochemical microscope at variable temperatures: simultaneous temperature and electrochemical imaging and its kinetic studies, *Sci. Rep.*, 2017, **7**(1), 43685, DOI: **10.1038/srep43685**.
35 L. Meng, J. G. Iacobini, M. B. Joseph, J. V. Macpherson and M. E. Newton, Laser heated boron doped diamond electrodes: effect of temperature on outer sphere electron transfer processes, *Faraday Discuss.*, 2014, **172**, 421–438, DOI: **10.1039/C4FD00044G**.
36 Y. Yu, J. D. Williams and K. A. Willets, Quantifying photothermal heating at plasmonic nanoparticles by scanning electrochemical microscopy, *Faraday Discuss.*, 2018, **210**, 29–39, DOI: **10.1039/C8FD00057C**.
37 S. Gutierrez-Portocarrero, P. Subedi and M. A. Alpuche-Aviles, Laser induced temperature perturbation on ultramicroelectrodes: unsupported solutions in nonaqueous methanol, *J. Electrochem. Soc.*, 2022, **169**, 016509, DOI: **10.1149/1945-7111/ac49ca**.